Flexible carbon nanotubes electrode for neural recording

Chia-Min Lin[a], Yu-Tao Lee[a], Shih-Rung Yeh[c], Weileun Fang[a,b,*]

[a] Institute of NanoEngineering and MicroSystems, National Tsing Hua University, Hsinchu 30013, Taiwan
[b] Department of Power Mechanical Engineering, National Tsing Hua University, Hsinchu 30013, Taiwan
[c] Institute of Molecular Medicine, National Tsing Hua University, Hsinchu 30013, Taiwan

ARTICLE INFO

ABSTRACT

This paper demonstrates a novel flexible carbon nanotubes (CNTs) electrode array for neural recording. In this device, the CNTs electrode arrays are partially embedded into the flexible Parylene-C film using a batch microfabrication process. Through this fabrication process, the CNTs can be exposed to increase the total sensing area of an electrode. Thus, the flexible CNTs electrode of low impedance is realized. In application, the flexible CNTs electrode has been employed to record the neural signal of a crayfish nerve cord for *in vitro* recording. The measurements demonstrate the superior performance of the presented flexible CNTs electrode with low impedance (11.07 kΩ at 1 kHz) and high peak-to-peak amplitude action potential (about 410 μV). In addition, the signal-to-noise ratio (SNR) of the presented flexible CNTs electrode is about 257, whereas the SNR of the reference (a pair of Teflon-coated silver wires) is only 79. The simultaneous recording of the flexible CNTs electrode array is also demonstrated. Moreover, the flexible CNTs electrode has been employed to successfully record the spontaneous spikes from the crayfish nerve cord. The amplitude of the spontaneous peak-to-peak response is about 25 μV.

© 2009 Elsevier B.V. All rights reserved.

1. Introduction

The response of neural cells is traditionally recorded by a glass electrode (Schanne et al., 1968). Various microelectrode arrays (MEAs) have been reported to measure the responses of neural cells. These MEAs can significantly increase the efficiency of neural signal recording (Egert et al., 1998), stimulating the neural cells (Hochberg et al., 2006), and they have been widely applied for neural prosthetic systems such as retinal implants (Zrenner, 2002), and cochlear implants (Wilson et al., 2003). In general, the dimension of neural cells ranges from several tens to several hundreds of micrometers. It is preferable to be able to easily modify the number of the electrode sites and the spacing between the electrode sites for different applications. In this regard, microfabrication technology is especially suitable to implement the MEA for neural applications.

Presently, various MEAs have been successfully demonstrated using microelectromechanical system (MEMS) technology. Typically, MEA can be classified as a planar type (Egert et al., 1998; Manos et al., 1999; Kim et al., 2007) and a probe type (Campbell et al., 1991; Griss et al., 2001; Norlin et al., 2002; Chu et al., 2006; Hochberg et al., 2006). The probe type MEA can easily penetrate biological tissues, and thus it is applied to *in vivo* recording (Hochberg

et al., 2006). On the other hand, the planar type MEA is usually applied for *in vitro* recording (Egert et al., 1998). In general, these MEAs are implemented using the Si-based (Campbell et al., 1991; Manos et al., 1999; Yoon et al., 2000; Griss et al., 2001; Norlin et al., 2002; Chu et al., 2006; Hochberg et al., 2006) and polymer-based (Kim et al., 2007) fabrication technologies. Since silicon is a brittle material, the Si-based MEA could be broken during biological tests. In this regard, the polymer material, which has higher flexibility and better bio-compatibility, is considered as a promising substrate material for MEA (Kim et al., 2007). Besides, the diamond MEA (Chan et al., 2008) has been reported recently due to its good mechanical strength, but a more complicated fabrication process is required. Since CNTs have many superior material properties, such as mechanical stability, chemical durability, good electrical conductance, large capacitance, and bio-compatibility, they are also employed to act as the electrode (Lovat et al., 2005). The CNTs electrodes have also been implemented on silicon substrate (McKnight et al., 2006; Gabay et al., 2007; Ben-Jacob and Hanein, 2008), quartz (Wang et al., 2006), glass coverslip (Mazzatenta et al., 2007), pyrex 7740 (Gabriel et al., 2008), and sharp tungsten probe (Keefer et al., 2008). In addition, the CNTs also have the advantage of increasing the sensing area of an electrode.

It is much easier to handle the flexible polymer film during neural recording (Kim et al., 2007). There are many existing techniques to integrate CNTs with flexible polymer substrate, for instance, low temperature growth (Chen et al., 2003; Shao et al., 2004), liquid polymer molding (Jung et al., 2006), direct mixing (Ci et al., 2008), microwave welding (Wang et al., 2007; Chen et al., 2008), and stamp

---

* Corresponding author at: Department of Power Mechanical Engineering, National Tsing Hua University, 101, Section 2, Kuang-Fu Road, Hsinchu 30013, Taiwan. Tel.: +886 3 574 2923; fax: +886 3 573 9372.
E-mail address: fang@pme.nthu.edu.tw (W. Fang).

transfer (Hur et al., 2005; Zhou et al., 2006); however, the low temperature growth CNTs (Chen et al., 2003; Shao et al., 2004) exhibit poor material properties (lower graphitization). In Jung et al. (2006) and Ci et al. (2008), the CNTs are wrapped in polymer film so that the sensing area can not be increased. Moreover, it is a challenge to pattern CNTs for the approaches in Wang et al. (2007), Ci et al. (2008) and Chen et al., 2008. The low temperature growth (Chen et al., 2003; Shao et al., 2004) and stamp transfer method (Hur et al., 2005; Zhou et al., 2006) have the problem of poor adhesion between CNTs and polymer film. To prevent the drawbacks of the existing approaches, this study has established a process to fabricate and integrate patterned CNTs and flexible polymer. Based on this process technology, the flexible CNTs electrode array (a planar type MEA) for neural recording is designed and implemented. In this device, the stiff and vertically aligned carbon nanotubes are partially embedded into the polymer film using microfabrication processes to form the flexible CNTs electrode arrays. To demonstrate the feasibility of the presented planar type MEA, the CNTs electrode array has been grown by the thermal furnace and patterned on a silicon substrate and then transferred onto a flexible Parylene-C film. The fabricated device has also been successfully employed to record the nerve cord response of crayfish.

2. Design concept and fabrication process

Fig. 1a shows the schematic illustrations of the presented flexible CNTs neural electrode design. As indicated in Fig. 1a (upper figure), this study employs the vertically aligned CNTs to form the components of the device, such as the sensing electrode sites, conducting wire, and bonding pads. Fig. 1a (lower figure) shows the cross section of AA' indicated in Fig. 1a (upper figure). As depicted in Fig. 1a (lower figure), some of these CNTs components are covered with dielectric material for electrical isolation during measurement. The CNTs offer the characteristics of mechanical stability, chemical durability, good electrical conductance, large capacitance, and bio-compatibility for these components. Moreover, the surface area of the sensing electrode can be increased by CNTs, and then the impedance of the electrode can be further decreased. As a result, the CNTs sensing electrode can increase the signal-to-noise ratio (SNR) to record better action potential. These vertically aligned CNTs structures are embedded into a polymer film to realize the flexible planar MEA. The Parylene-C polymer film is used in this study for its promising properties of chemical inertness, class-VI (USP) implantable plastic material, and bio-compatibility. Since the Parylene-C film is transparent, the bio-tissue under the presented flexible MEA can be clearly observed during the test. In addition, the pattern of CNTs electrode arrays and their integration with Parylene-C polymer film can be easily implemented using microfabrication processes.

This study established the fabrication process, as shown in Fig. 1b, to realize the presented design illustrated in Fig. 1a. First, the oxide and poly-silicon films were deposited to respectively act as the etch stop layer and device released layer. After photolithography, the 5 nm thick *Fe*-film was deposited and patterned by lift-off technology onto Si-substrate to act as the catalyst film for the growth of CNTs, as shown in step I (Fig. 1b). The in-plane shapes of the electrode site, conducting wire, and bonding pad were defined in this step. As illustrated in step II (Fig. 1b), the vertically aligned carbon nanotubes of 100 μm in height were grown via pyrolysis of acetylene at 800 °C in an Ar/NH₃ flow for 15 min to form the structures of the electrode site, conducting wire, and bonding pad. As shown in step III (Fig. 1b), the chemical vapor deposition (CVD) Parylene-C was then deposited onto the silicon substrate with patterned CNTs at room temperature. This was the most critical step for the presented processes. The thickness of the flexible polymer

layer in Fig. 1a was determined by this CVD process. Moreover, the CVD Parylene-C film was also employed to fill into the gap of aligned CNTs to reinforce the intertube binding (Fang et al., 2005; Hsu et al., 2008). In general, the conformal coverage CVD process allows parylene to fill into the gap between the CNTs for a thickness of 8 μm, which provides a reasonable binding strength for the discrete CNTs. The device chip was then bonded with the handle wafer (pyrex 7740 glass) by the double-sided thermal release tape, as illustrated in step IV (Fig. 1b). After that, the polysilicon was finally etched by XeF₂, and devices were peeled off from the substrate, as shown in step V (Fig. 1b). The polydimethylsiloxane (PDMS) polymer was dispensed (by a commercial pneumatic dispensing system, Ultra™ 2400 series of EFD Inc.) onto part of the CNTs to act as the insulation layer (Lee et al., 2006). Finally, the device was heated on the hot plate at 120 °C to solidify the PDMS, and then peeled off from the double-sided thermal release tape, as indicated in step VI (Fig. 1b). As a result, the CNTs components were bound tightly on a flexible parylene film. The CNTs of the electrode site, as indicated in Fig. 1a (lower figure), were exposed to increase the total sensing area, and the impedance of the electrode was lowered. The processes shown in Fig. 1b can be batch fabricated on silicon substrate. Thus, the flexible CNTs sensing electrode arrays of small and arbitrary patterns can be batch fabricated on a substrate.

3. Results and discussions

3.1. Micro fabrication results

The scanning electron microscope (SEM) micrographs in Fig. 2 show typical fabrication results. The CNTs of 100 μm in height can be observed from the side-view micrograph of Fig. 2 (upper figure). The alignment of CNTs is highlighted by zoom-in micrograph in Fig. 2 (upper figure). Fig. 2 (lower figure) shows the CNT-polymer composites after the CVD of Parylene-C film. The photo in Appendix B Supplementary Fig. S1a displays 2 × 2 carbon nanotube electrode arrays prior to the removal of Si-substrate, and the patterns denote the structures consist of CNTs. Appendix B Supplementary Figs. S1b and S1c respectively show the 2 × 2 and 2 × 1 CNTs electrode arrays on the free standing flexible Parylene-C film. The parylene film is 36 μm thick for both of these two cases. The transparent and opaque regions represent the parylene film and CNT-parylene composites, respectively. The photo in Appendix B Supplementary Fig. S2 shows that the bending of polymer film demonstrates the flexibility of the presented device. Finally, the photo in Fig. 3 shows the complete test unit of flexible 2 × 1 CNTs electrode arrays after wire bonding. The contact area of the bonding pad and conducting wire were passivated by UV (ultraviolet)-curable glue and PDMS, respectively. As to the dimensions of the flexible CNTs electrode, the opening area of the electrode site is 1962.5 μm², and the length of the conducting wire is 8100 μm. The current–voltage (I–V) property of the device was characterized using a two-terminal probe, as shown in Appendix B Supplementary Fig. S3. The results yield a linear I–V curve with a resistance of 1.69 kΩ, and also indicate the ohmic conduction property and the minimization of intertube scattering within the device.

3.2. Characterization of CNTs

The transmission electron microscopic (TEM) image of CNTs grown on *Fe* catalyst is shown in Appendix B Supplementary Fig. S4a, hence the multi-wall structure and the compartmentalized structure of CNTs are clearly observed. The diameter of multi-wall CNTs ranges from 30 nm to 40 nm. Appendix B Supplementary Fig. S4b shows the Raman spectrum of CNTs centered at 1350 cm⁻¹ (D band) and 1575 cm⁻¹ (G band), respectively. The relative intensity
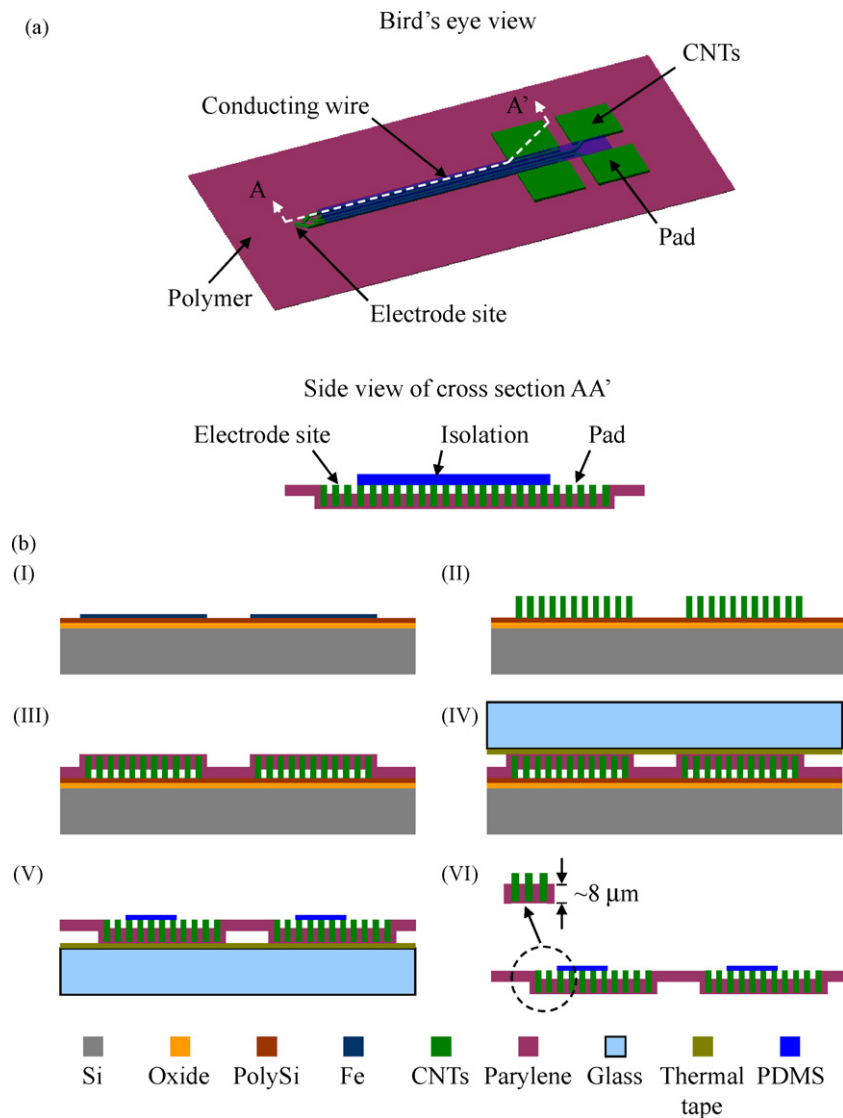
Fig. 1. Scheme of the flexible CNTs electrode (a) the bird's eye view of the device and the side-view of cross section AA', and (b) the fabrication process steps.

of the D band (named I_D) represents the degree of disordered CNTs structure, and a smaller I_D indicates fewer defects in CNTs structure (e.g. the 5- and 7-rings into hexagonal networks). In addition, the relative intensity of the G band (named I_G) represents the degree of graphitic CNTs structure, and a larger I_G indicates the complete graphitic structure of CNTs. Thus, the intensity ratio of I_D/I_G can be used to determine the graphitization of CNTs. As the disordered structure increases in nanotubes, the electrical conduction of CNTs film would decrease by the presence of electron scattering (Heer et al., 1995; Avouris, 2002; Hayashi et al., 2006; Lan et al., 2007). In this study, the CNTs were grown by a high temperature CVD process, and the CNTs structure was well graphitized. As shown in Appendix B Supplementary Fig. S4b, the ratio of I_D/I_G was 0.7. In comparison, the I_D/I_G ratio of the low temperature growth CNTs ranges from 0.9 to 1.3 (Chen et al., 2003; Shao et al., 2004). As a result, the presented CNTs electrode has better electrical conduction, and is more appropriate for the application of neural recording.

3.3. Electrical/electrochemical characterization of flexible CNTs electrode

The experimental setup in Appendix B Supplementary Fig. S5 was established to characterize the impedance of the fabricated flexible CNTs electrode. The flexible CNTs electrode served as the working electrode, and the Ag/AgCl coil acted as the reference electrode. Both of these two electrodes were immersed into a phosphate-buffered saline (PBS, pH 7.4) solution. The impedance analyzer (HP 4284) was employed to apply an alternating current (AC) of 30 mV at swept-frequency of 50 Hz to 10 kHz to these two electrodes. In the first case, the whole flexible CNTs electrode (including the electrode site, the conducting wire, and the bonding pads) was fully immersed into the PBS solution. The measurement results in Fig. 4 show the variation of impedance and phase at different frequencies; and the measured impedance is 11.07 kΩ (with a phase shift of −10.59°) at 1 kHz which is the typical frequency for neural recording. As a comparison, in the second test, only the electrode site of the flexible CNTs electrode was immersed into a PBS solution. The experiment results indicated that the measured impedance of the second case remained unchanged. Thus, it shows that the CNTs conducting wire and the bonding area were successfully isolated by the PDMS and UV-curable glue passivation layers, respectively. As compared with the existing researches (Norlin et al., 2002; Kim et al., 2007; Chan et al., 2008), the presented flexible CNTs electrode provides smaller impedance. Moreover, the two-electrode system in Appendix B Supplementary Fig. S5 was also employed to characterize the electrochemical property of the
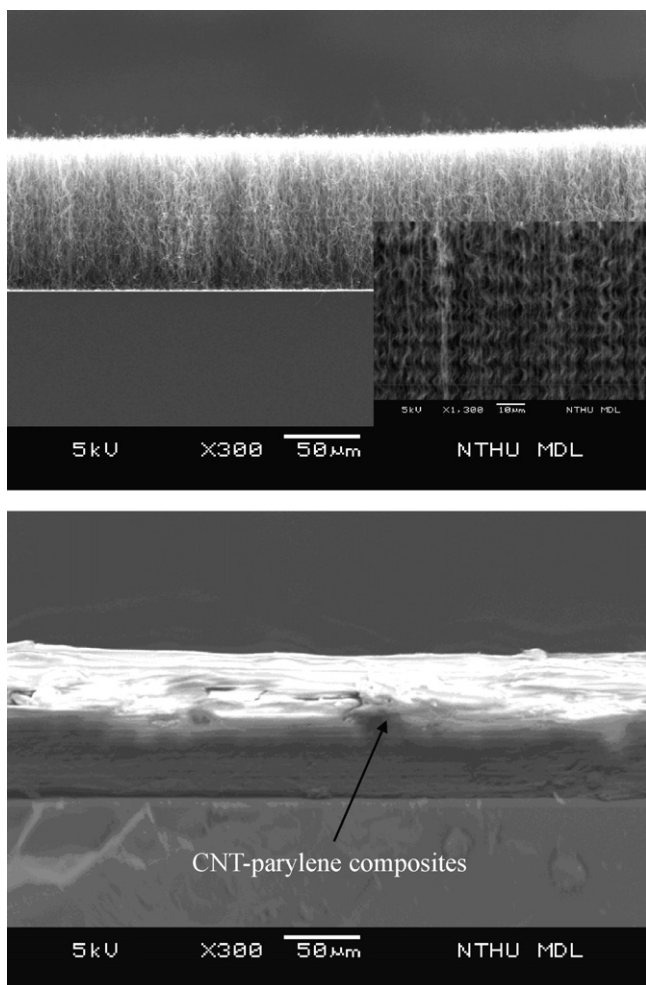
Fig. 2. The SEM micrographs of fabrication results, (upper figure) side-view of vertically aligned CNTs and zoom-in of vertically aligned CNTs, and (lower figure) concrete of vertically aligned CNTs and Parylene-C.

CNTs electrode. As described below, the flexible CNTs electrode and the Ag/AgCl coil acted as the working and reference electrodes, respectively. The measurement instrument (Keithley 2602) was connected with these two electrodes through the Labview control, and the cyclic voltammograms (CV) were measured as shown in Appendix B Supplementary Fig. S6a. The potential window ranges
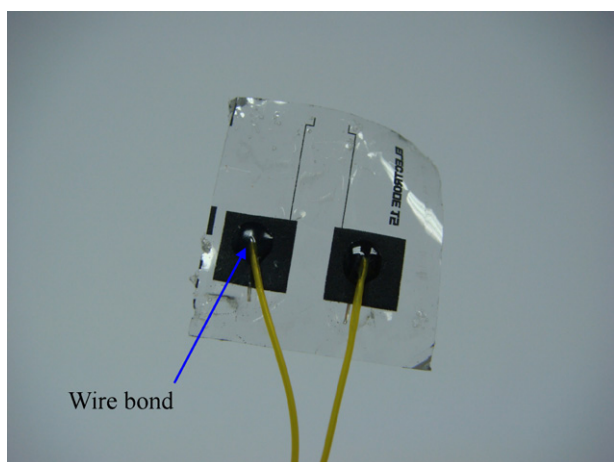
Fig. 3. Photo of the transparent flexible CNTs electrode after wire bond.
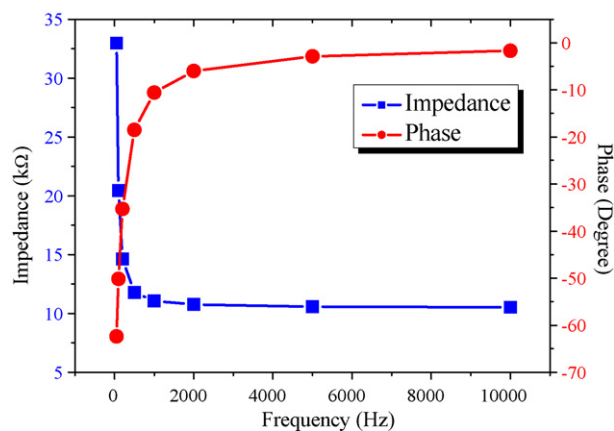
Fig. 4. Variation of impedance and phase with input frequencies, as the presented flexible CNTs electrode measured in PBS.

from −0.3 V to 0.7 V, and there is no oxygen and hydrogen evolution within this range. Appendix B Supplementary Fig. S6b further shows the oxidation current Δi versus the scan rate dV/dt. Since interface capacitance C of the electrode site is expressed as (Gabay et al., 2007),

$$C = \left(\frac{1}{2}\right) \times \left(\frac{\Delta i}{dV/dt}\right) \tag{1}$$

thus, the interface capacitance of the presented CNTs electrode is $C = 232.23$ nF.

3.4. Biological test of flexible CNTs electrode

The packaged device, as shown in Fig. 3, was also employed to record the action potential of a crayfish nerve cord to evaluate the performance of a flexible CNTs electrode array. As shown in Fig. 5, the flexible 2×1 CNTs was pinned on the Petri dish to record the spikes from the crayfish nerve cord. Two commercial Teflon-coated silver-wires respectively acted as stimulation and reference electrodes. The zoom-in photo in Fig. 5 further shows the CNTs, stimulation, and reference electrodes. The entire experimental setup, as shown in Appendix B Supplementary Fig. S7, was mounted on the stage of a microscope, and the stimulation and reference electrodes were precisely positioned using the micromanipulator. To prepare the test sample, the adult crayfish was placed in ice-cold water to reduce motion and muscle contraction during dissection. The crayfish was then pinned with its dorsal-side upwards, and the nerve cord at the ventral-side was exposed after removal of the exoskeleton and muscle. During the dissection, the crayfish was immersed in the van Harreveld's solution. Appendix B Supplementary Fig. S8b shows the cross sections of the crayfish nerve cord indicated in Fig. S8a. The XX' cross section in Fig. S8b indicates the crayfish nerve cord consists of six abdominal segments (Ab1–Ab6). As indicated in the YY' cross section of Fig. S8b, each segment contains four giant axons (two lateral giant axons, named LG; and two medial giant axons, named MG) at the dorsal-side, and many interneurons at the ventral-side. During the experiment, the two CNTs electrodes shown in Fig. 5 were in contact with the LG at the Ab2 and Ab3 segments of nerve cord, as illustrated in Appendix B Supplementary Fig. S8b. Moreover, a pair of Teflon-coated silver wires was placed on the Ab1 segment of the nerve cord as a stimulation electrode to excite the giant axon. Another pair of Teflon-coated silver wires, which acted as a reference electrode to simultaneously record the spikes with the flexible CNTs electrode, was placed on the Ab5 segment of nerve cord.

To stimulate the giant axon, a square pulse was generated from the digital-to-analog card (DAC) (PCI-1602 ICP, DAS, Taiwan), and
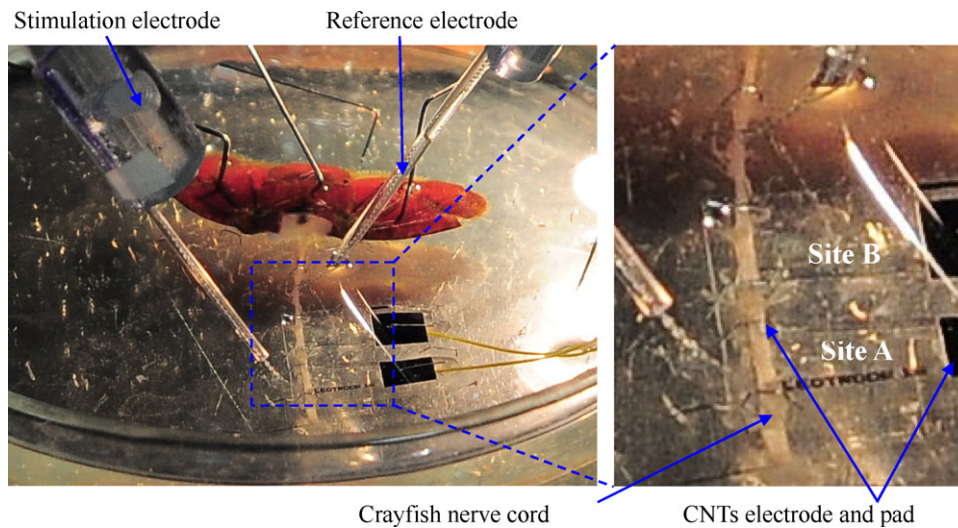
Fig. 5. The zoom-in photos of the experimental setup for neural recording of the crayfish nerve cord (the entire experiment setup is shown in Appendix B Supplementary Fig. S7). The left photo shows the crayfish inside the Petri-dish; the flexible 2 × 1 CNTs electrode, and the stimulation and reference electrodes (Teflon-coated silver wires) in contact with the crayfish nerve cord. The right photo further shows the crayfish nerve cord with the transparent flexible 2 × 1 CNTs electrode (marked with Site A and Site B).

the waveform (amplitude, pulse duration, and period) of the square pulses were controlled by a computer program (developed by the Brain Research Center, National Tsing Hua University, Taiwan). The recorded signal was amplified with a gain of 1000 by the AC differential amplifier (A-M systems Model 1700). The high-pass and low-pass filters were employed to attenuate the unwanted signals. The cut-off frequencies of the high-pass and low-pass filters were 0.5 Hz and 5 kHz, respectively. The amplified signals were recorded onto the computer with a sampling frequency of 200 kHz. The crayfish nerve cord was stimulated by a square pulse (amplitude of 7 V, and pulse duration of 0.1 ms) every 5 ms during the test, and then the action potential was recorded by the presented CNTs electrode and the reference electrode. Appendix B Supplementary Fig. S9 shows the typical responses of the crayfish nerve cord recorded from the flexible CNTs electrode (Site A) within 60 ms, the action potential of crayfish nerve cord was constantly generated after the electrical stimulation given by the stimulation electrode. Fig. 6a further indicates the measured signal of the crayfish nerve cord ranging from 9 ms to 16 ms. In this study, the all-or-none behavior of action potential was employed to confirm that the recorded spike was not an artifact. First, the stimulation voltage was started at 2 V and then increased by 0.1 V at each step to find the threshold voltage to excite the giant axon. The spike was not generated until a threshold voltage of 7 V was reached. After that, the stimulation voltage was started at 8 V and then decreased by 0.1 V at each step to confirm the threshold voltage of 7 V. As the voltage was a bit smaller than the threshold voltage of 7 V, the spike was not generated. Such all-or-none behavior of action potential rules out the possibility of an artifact signal. The amplitude of the measured action potential is about 410 μV peak to peak (Solid line), and the time interval between the artifact signal and action potential is about 0 ms–1 ms. In the meantime, the response of the crayfish nerve cord was also recorded by the reference electrode (Teflon-coated silver wire) (Dashed line). As a comparison, the signals recorded by the flexible CNTs electrode (Site A) (Solid line) and the reference electrode (Dashed line) are shown in Fig. 6a. As indicated in Fig. 5, the flexible CNTs electrode (Site A) was placed closer to the stimulation electrode. Since the action potential was generated at the Ab1 segment and then transmitted to the Ab6 segment, the signal recorded by the reference electrode had a time delay comparable to the CNTs electrode. The amplitude of the action potential recorded by the reference electrode was about 143 μV peak to peak. As a result, the amplitude of action potential of the CNTs electrode was 2.9-fold
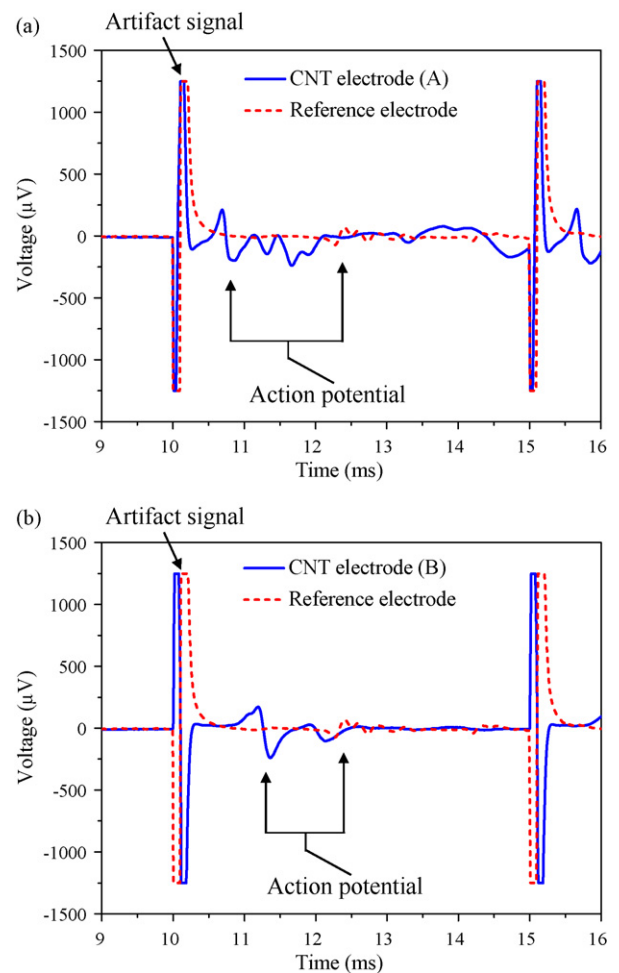
Fig. 6. The neural responses of crayfish nerve cord recorded by the presented flexible 2 × 1 CNTs electrode and reference electrode (Teflon-coated silver wires), (a) zoom-in of the first action potential recorded by CNTs electrode in Appendix B Supplementary Fig. S9 (at Site A) and reference electrode, and (b) action potential recorded by CNTs electrode (at Site B) and reference electrode.

higher than that of the reference electrode. The SNR of the flexible CNTs electrode was as high as 257, whereas the SNR of the reference electrode was only 79. The SNR was defined as the ratio of the peak to peak amplitude of action potential measured in Fig. 6a to the root mean square (rms) value of background noise (Yoon et al., 2000). Fig. 6b shows the measured signal of the crayfish nerve cord from the other electrode (Site B). According to the results in Fig. 6a and b, the array signal can be simultaneously recorded by the flexible 2×1 CNTs electrode.

Moreover, the flexible CNTs electrode was also successfully employed to record the spontaneous spikes from the crayfish nerve cord. Spontaneous spikes were generated from the interneurons in the ganglion of the abdominal nerve cord. The interneurons were located in the ventral-side of the nerve cord. Since the flexible CNTs electrode was placed at the dorsal-side of the nerve cord, which is not in direct contact with the signal source, the amplitude of the action potential is much smaller than the lateral giant (LG) signal. Appendix B Supplementary Fig. S10a shows the typical recorded signal for 400 ms. Appendix B Supplementary Fig. S10b further indicates the measured signal ranging from 150 ms to 160 ms, and the amplitude of the spontaneous response was about 25 μV peak to peak. The high SNR (with a number of 17) recording in Appendix B Supplementary Fig. S10b demonstrates the superior recording ability of a flexible CNTs electrode in this study, and implicates a promising multi-electrode array for *in vivo* recording in the future.

4. Conclusions

This study has successfully demonstrated a novel flexible CNTs electrode to act as a planar MEA for neural recording. Fabrication was based on a four-step simple process including carbon nanotube growth, polymer binding, flexible film transformation, and partial isolation. The fabrication processes of this study can be batch fabricated on silicon substrate. Thus, the flexible CNTs sensing electrode arrays of small and arbitrary patterns can be batch fabricated on a substrate. Through CVD polymer deposition, CNTs can be bound with the polymer film. Moreover, the CNTs at the electrode site remain exposed to the ambient. The total sensing area of the electrode is increased and the impedance of MEA is decreased. Testing of the flexible CNTs electrode on the crayfish nerve code was also performed. As a result, the impedance of the presented flexible CNTs electrode is 11.07 kΩ at 1 kHz which is the typical frequency for neural recording. This value is one to two orders of magnitude smaller than those measured using the existing MEAs, and thus significantly improves the performance of the neural electrode. The crayfish nerve cord was connected compactly by the presented flexible device when recording. A better SNR of 257 is also demonstrated, whereas the SNR of the reference electrode is only 79. In summary, the presented flexible CNTs electrode has many advantages as compared with the existing non-CNT MEAs (such as Si-based and polymer-based micromachined MEAs): (1) Simple fabrication process: the conventional MEMS based technology MEA was usually implemented using the complicated multi-layer thin film process (Yoon et al., 2000; Norlin et al., 2002; Kim et al., 2007; Chan et al., 2008), whereas the flexible CNTs electrode was fabricated by a simple process in Fig. 1b; (2) Flexible device: the fragile Si-based MEA has the broken issue (Campbell et al., 1991; Manos et al., 1999; Griss et al., 2001; Norlin et al., 2002; Chu et al., 2006; Hochberg et al., 2006); on the other hand, the polymer-based flexible CNTs electrode can be adhered along the bio-tissue during testing (Kim et al., 2007); (3) Low impedance: the CNTs electrode has smaller impedance than the conventional MEMS based MEA with Au or Pt as the electrode site, and this impedance value is one to two orders of magnitude smaller than conventional MEMS based MEAs (Norlin et al., 2002; Kim et al., 2007; Chan et al., 2008); and (4) Smaller parasitic capacitance: The isolation layers of MEA (parylene-C, PDMS,

SiO_2, Si_3N_4) are in contact with the liquid buffer (PBS) and induce parasitic capacitances. In general, the dielectric constants of the polymer-based MEA (dielectric constant of parylene-C: 3.15; dielectric constant of PDMS: 2.3~2.8) and the Si-based MEA (dielectric constant of SiO_2: 2.8; dielectric constant of Si_3N_4: 7.8) are the same order of magnitude. However, the parylene-C layer (36 μm) of the presented flexible CNTs MEA is much thicker than the isolation layer (such as SiO_2, and Si_3N_4) of the Si-based MEA. Thus, the presented device has smaller parasitic capacitances.

Despite the aforementioned advantages, the presented flexible CNTs electrode still has some drawbacks. Presently, the neural signal detected by the presented flexible CNTs electrode must be processed (amplifying, filtering, and digital-to-analog converting) by a bulky instrument (A-M systems Model 1700). This requirement creates limitations during the applications of the flexible CNTs electrode. In this regard, the flexible CNTs electrode will be further integrated with the CMOS circuit chips containing an amplifier, digital-to-analog converter, etc. (Li et al., 2008). The superior recording ability of the flexible CNTs electrode could find other biological applications. For instance, the *in vivo* micro-probe can be employed to record brain neural signals and reduce trauma during long-term implants. It is easy for the flexible parylene substrate to fit the diverse shapes of the human body (for instance, the wrist, knee, eye, skull, and chest), and thus the flexible CNTs electrode can find more applications by recording other kinds of electrical signals (EMG, EOG, EEG, or ECG).

Acknowledgements

Appendix A. Supplementary data

Supplementary data associated with this article can be found, in the online version, at doi:10.1016/j.bios.2009.02.005.

References

Avouris, P., 2002. Chemical Physics 281, 429–445.
Ben-Jacob, E., Hanein, Y., 2008. Journal of Materials Chemistry 18, 5181–5186.
Campbell, P.K., Jones, K.E., Huber, R.J., Horch, K.W., Normann, R.A., 1991. IEEE Transactions on Biomedical Engineering 38, 758–768.
Chu, H.-Y., Kuo, T.-Y., Chang, B., Lu, S.-W., Chiao, C.-C., Fang, W., 2006. Sensors and Actuators A 130–131, 254–261.
Chan, H.-Y., Aslam, D.M., Wang, S.H., Swain, G.M., Wise, K.D., 2008. IEEE 21st International Conference on MEMS, Tuscon, USA, pp. 244–247.
Chen, M., Chen, C.-M., Shi, S.-C., Chen, C.-F., 2003. Japanese Journal of Applied Physics 42, 614–619.
Ci, L., Suhr, J., Pushparaj, V., Zhang, X., Ajayan, P.M., 2008. Nano Letters 8, 2762–2766.
Chen, T.-H., Tsai, T.-Y., Hsieh, K.-C., Chang, S.-C., Tai, N.-H., Chen, H.-L., 2008. Nanotechnology 19, 465303.
Egert, U., Schlosshauer, B., Fennrich, S., Nisch, W., Fejtl, M., Knott, T., Muller, T., Hammerle, H., 1998. Brain Research Protocols 2, 229–242.
Fang, W., Chu, H.-Y., Hsu, W.-K., Cheng, T.-W., Tai, N.-H., 2005. Advanced Materials 17, 2987–2992.
Griss, P., Enoksson, P., Tolvanen-Laakso, H.K., Meriläinen, P., Ollmar, S., Stemme, G., 2001. Journal of Microelectromechanical Systems 10, 10–16.
Gabay, T., Ben-David, M., Kalifa, I., Sorkin, R., Abrams, Z.R., Ben-Jacob, E., Hanein, Y., 2007. Nanotechnology 18, 035201.
Gabriel, G., Gómez, R., Bongard, M., Benito, N., Fernández, E., Villa, R., 2008. Biosensors and Bioelectronics, 036, doi:10.1016/j.bios.2008.09.

Hochberg, L.R., Serruya, M.D., Friehs, G.M., Mukand, J.A., Saleh, M., Caplan, A.H., Branner, A., Chen, D., Penn, R.D., Donoghue, J.P., 2006. Nature 442, 164–171.

Hur, S.-H., Park, O.O., Rogers, J.A., 2005. Applied Physics Letters 86, 243502.

Hsu, W.-K., Chu, H.-Y., Chen, T.-H., Cheng, T.-W., Fang, W., 2008. Nanotechnology 19, 135304.

Heer, W.A.d., Bacsa, W.S., Châtelain, A., Gerfin, T., Humphrey-Baker, R., Forro, L., Ugarte, D., 1995. Science 268, 845–847.

Hayashi, Y., Tokunaga, T., Kaneko, K., Horita, Z., 2006. Diamond and Related Materials 15, 1138–1142.

Jung, Y.J., Kar, S., Talapatra, S., Soldano, C., Viswanathan, G., Li, X., Yao, Z., Ou, F.S., Avad-hanula, A., Vajtai, R., Curran, S., Nalamasu, O., Ajayan, P.M., 2006. Nano Letters 6, 413–418.

Kim, Y.-H., Lee, C., Ahn, K.M., Kim, Y.-J., Lee, M., 2007. Sensors and Actuators A 139, 58–65.

Keefer, E.W., Botterman, B.R., Romero, M.I., Rossi, A.F., Gross, G.W., 2008. Nature Nanotechnology 3, 434–439.

Lovat, V., Pantarotto, D., Lagostena, L., Cacciari, B., Grandolfo, M., Righi, M., Spalluto, G., Prato, M., Ballerini, L., 2005. Nano Letters 5, 1107–1110.

Lee, S.-Y., Tung, H.-W., Chen, W.-C., Fang, W., 2006. IEEE Photonics Technology Letters 18, 2191–2193.

Lan, C., Amama, P.B., Fisher, T.S., Reifenberger, R.G., 2007. Applied Physics Letters 91, 093105.

Li, W., Rodger, D.C., Tai, Y.C., 2008. IEEE 21st International Conference on MEMS, Tuscon. USA, pp. 108–111.

Manos, P., Pancrazio, J.J., Coulombe, M.G., Ma, W., Stenger, D.A., 1999. Neuroscience Letters 271, 179–182.

McKnight, T.E., Melechko, A.V., Fletcher, B.L., Jones, S.W., Hensley, D.K., Peckys, D.B., Griffin, G.D., Simpson, M.L., Ericson, M.N., 2006. Journal of Physical Chemistry B 110, 15317–15327.

Mazzatenta, A., Giugliano, M., Campidelli, S., Gambazzi, L., Businaro, L., Markram, H., Prato, M., Ballerini, L., 2007. Journal of Neuroscience 27, 6931–6936.

Norlin, P., Kindlundh, M., Mouroux, A., Yoshida, K., Hofmann, U.G., 2002. Journal of Micromechanics and Microengineering 12, 414–419.

Schanne, O.F., Lavallee, M., Laprade, R., Gagne, S., 1968. Proceedings of the IEEE 56, 1072–1082.

Shao, M., Wang, D., Yu, G., Hu, B., Yu, W., Qian, Y., 2004. Carbon 42, 183–185.

Wilson, B.S., Lawson, D.T., Müller, J.M., Tyler, R.S., Kiefer, J., 2003. Annual Review of Biomedical Engineering 5, 207–249.

Wang, K., Fishman, H.A., Dai, H., Harris, J.S., 2006. Nano Letters 6, 2043–2048.

Wang, C.Y., Chen, T.H., Chang, S.C., Chin, T.S., Cheng, S.Y., 2007. Applied Physics Letters 90, 103111.

Yoon, T.H., Hwang, E.J., Shin, D.Y., Park, S.I., Oh, S.J., Jung, S.C., Shin, H.C., Kim, S.J., 2000. IEEE Transactions on Biomedical Engineering 47, 1082–1087.

Zrenner, E., 2002. Science 295, 1022–1025.

Zhou, Y., Hu, L., Grüner, G., 2006. Applied Physics Letters 88, 123109.